LA-7432-MS
Informal Report

C.3

Shear-Layer Instability in Cylindrical Implosions of Rotating Fluids

University of California

LOS ALAMOS SCIENTIFIC LABORATORY
Post Office Box 1663 Los Alamos, New Mexico 87545

UNITED STATES
DEPARTMENT OF ENERGY
CONTRACT W-7405-ENG. 36

LA-7432-MS
Informal Report

Special Distribution
Issued: August 1978

Shear-Layer Instability in Cylindrical Implosions of Rotating Fluids

R. C. Mjolsness
H. M. Ruppel

SHEAR-LAYER INSTABILITY IN CYLINDRICAL IMPLOSIONS OF ROTATING FLUIDS

by

R. C. Mjolsness and H. M. Ruppel

ABSTRACT

One-dimensional implosions of a fluid in differential rotation and containing a steep shear layer have been studied numerically using an angular momentum conserving code. Some of the details of the code are presented. It is found that after the passage of the first radial shock, the pressure and velocity profiles oscillate about a power law close to that of a self-similar solution. The traveling oscillations are produced by the dynamics of a series of radial shocks. An approximate stability theory for the shear-layer instability is given for this geometry. It is found that growth rates increase very strongly as the implosion proceeds and that the details of the velocity profiles influence both the most unstable mode number and the absolute growth rate.

I. INTRODUCTION

It has been conjectured that the vorticity amplification of shear-layer instabilities during implosions may be of importance to implosion dynamics. One consideration is that angular momentum conservation requires that a tangential flow be amplified during the implosion. A second consideration is the very suggestive approximate analysis of Greenspan and Benney[1] in which it is shown that a time-dependent shear layer can have growth rates many times larger than that of the time-averaged shear layer. For implosions, both the contracting length scale and the radial shocks provide time dependences to the parameter appearing in the perturbation theory.

Following this line of investigation we have considered several effects:

(1) As the geometric scale of the imploding system decreases, the hydrodynamic instability e-folding time decreases even faster. In some systems linear compressions of more than an order of magnitude are contemplated and the contraction of e-folding time scales would be most severe. Thus a perturbation that seemed stable (i.e., very slowly growing) at early times, as displayed by a Phermex picture, might well be highly unstable at late times, as suggested by Pinex results.

(2) Both linear theory and crude modeling of nonlinear effects suggest that the m value of the most unstable perturbation may be highly time dependent. Thus a given mode may actually be stable for a substantial fraction of the implosion and then grow explosively near maximum compression. This could happen even for low m values (e.g., m = 2), possibly giving rise to gross disruptions of the system.

(3) It is possible that significant mixing of fluids and shells may turn out to be driven by hydrodynamic instabilities. The Rayleigh-Taylor instability has been mentioned most often in this connection, but other instabilities are also possibilities.

Actually, at least three instabilities are of possible interest in the weapons context: the Rayleigh-Taylor instability, the Helmholtz instability, and the vortex-stretching instability. Only the Rayleigh-Taylor instability has been extensively discussed in this connection and, even so, much remains to be learned about the effects of this instability. However, the numerous deviations of an actual implosion from an idealized radial implosion (e.g., non-ideal alignment of shells, non-perfect machining of a system, HE initiated at a discrete set of points and non-homogeneous burn of HE) mean that secondary, azimuthal flows can be generated in the system and these, in turn, can drive both the Helmholtz and the vortex-stretching instability.

In this work we report on the first stages of a program to explore these possibilities. We confine our attention to the Helmholtz instability and, to facilitate the comparison between analytical and numerical results and to simplify the analysis, we work only in cylindrical geometry. In addition, we work only with shear flows generated by a particular class of azimuthal velocity profiles that are simpler both analytically and physically than the general profile. In the following section we outline our present views on the likely sequence of development of such instabilities. In the subsequent sections we describe the first stages of what seems to be a verification of these views.

II. SUGGESTED DEVELOPMENT OF HELMHOLTZ INSTABILITY FOR CYLINDRICAL IMPLOSIONS WITH ANGULAR MOMENTUM

The principal result of linear theory of the Helmholtz instability in a cylindrical system in which the shear layer is provided by differential rotation is that the properties of the instability are remarkably similar to those of the plane geometry Helmholtz instability. Thus we may anticipate that the unstable disturbance will tend to roll up into a ring of vortex tubes parallel to the axis and in the vicinity of the shear layer. The vortex tubes alter the time-averaged properties of the shear layer and thus change the range of the most unstable values for subsequent instabilities during the course of the implosion. In particular the tubes, being of like algebraic sign of vorticity, will amalgamate, leaving fewer, larger, and stronger vortices. This thickens the effective shear layer and favors low m values for the most unstable subsequent disturbances as the implosion proceeds.

The purely linear theory of this disturbance indicates that the e-folding time of the instability will contract greatly during the course of the implosion. In addition, the most unstable wavelengths will be significantly affected by time variations in the ratio of (thickness of the shear layer)/(radius of the shear layer). The effect should be rather similar to that found in a plane geometry calculation of Greenspan and Benney, in which it was found that certain modes would be stable for a long while and then grow explosively at an order of magnitude faster growth rate than expected from time-independent driving conditions. In addition, the nonlinear effects should force the growth toward low m values near the maximum growth rates at maximum compression, as outlined previously.

The equations for perturbed quantities, expressed in a dimensionless time variable nonlinear in the physical time, contain one time-varying parameter, whose values are strongly influenced by the passage of the radial shocks described below. The instability equations will to first approximation have qualitative properties similar to those of a second-order differential equation with periodic (more probably, quasiperiodic) coefficients. We might anticipate that the qualitative behavior of solutions might resemble those of the simplest such equation, the Mathieu equation. If so, then there should be a stabilization of certain m values from the time dependence of the coefficients. If control over the implosion process can stabilize a range of m values near the most unstable ones (with constant coefficients) then there will be a "dynamic stabilization" similar to

that proposed for the Rayleigh-Taylor instability or for the stabilization of flute-like modes in MHD configurations.

III. THE VELOCITY PROFILE AND ITS SCALING LAWS

Azimuthal velocity profiles that are piecewise of the form

$$v(r,t) = \Omega(t)r + L(t)r^{-1} + v_o(t)$$

have certain simplicities not present in more general profiles and are dealt with here. Specifically, they do not generate viscous forces and are thus a) the natural result when a rotating system comes partially to equilibrium and b) profiles that lead to angular momentum conservation for each volume of fluid under radial implosions. Moreover, as shown below, these profiles are approximately preserved in a self-similar way under a radial implosion. Finally, these profiles do not generate vorticity in a perturbing flow for the basic configuration; accordingly the perturbation may be described by a scalar potential.

Therefore we construct a velocity profile for a flow that is rigidly rotating for $r < R(t) - h(t)$, contains a shear layer from $R(t) - h(t) < r < R(t) + h(t)$, and has constant angular momentum per unit mass for $R(t) + h(t) < r < a(t)$, where $a(t)$ gives the location of a free-slip wall, according to the rules

$$v(r,t) = \Omega_-(t)r \qquad \text{for } r \leq R(t) - h(t) ,$$

$$= \Omega(t)\left\{r - \frac{[R^2(t)-h^2(t)]}{r}\right\} \qquad \text{for } R(t)-h(t) \leq r \leq R(t) + h(t) \quad , \text{ and}$$

$$= \frac{L(t)}{r} \quad , \qquad \text{for } R(t) + h(t) \leq r \leq a(t) ,$$

where the functions of time will be further specified below. It is this profile that is studied in the analytic work and used as an initial condition in the numerical studies.

We require that the azimuthal velocity be $-v_o$ at R-h and $+v_o$ at R+h (generating the shear layer). Thus the time-dependent functions are related by

$$\Omega_-(t) = \frac{-v_o(t)}{[R(t)-h(t)]} \quad , \quad \Omega(t) = \frac{v_o(t)}{2h(t)} \quad , \text{ and} \quad L(t) = v_o(t)\ [R(t)+h(t)] \quad .$$

When the assumed self-similar velocity profile is combined with the requirements of angular momentum conservation it is found that the time dependences of all parameters of the velocity profile are determined by a single function of time, say R(t). The parameters are related by

$$a(t) = a(0)\left[\frac{R(t)}{R(0)}\right], \qquad h(t) = h(0)\left[\frac{R(t)}{R(0)}\right],$$

$$L(t) = L(0), \qquad v_o(t) = v_o(0)\left[\frac{R(0)}{R(t)}\right],$$

$$\Omega_-(t) = \Omega_-(0)\left[\frac{R(0)}{R(t)}\right]^2, \text{ and } \Omega(t) = \Omega(0)\left[\frac{R(0)}{R(t)}\right]^2.$$

It turns out in the numerical studies that these scalings are approximately realized. Hence the velocity profile is approximately preserved during the course of an implosion.

IV. RADIAL IMPLOSION OF ROTATING ADIABATIC GAS

The Euler equations for an adiabatic gas of initial azimuthal velocity profile as given in the previous section are discretized using an angular momentum conserving code. This code, which was written in collaboration with Francis H. Harlow, is written in polar coordinates with radial and azimuthal velocities positioned at cell edges. The theta (azimuthal) coordinate is labeled with i, the radial coordinate with j. Within the constraint that i-lines be straight radial lines and that all vertices on a given j-line lie at a single distance from the origin (though this distance can change from cycle to cycle), the mesh is allowed to follow the fluid flow. In common with the ALE[2] approach, on which the fluxing scheme is modeled, we can permit not only variable resolution, but a movable mesh to follow the regions of interest. Such a scheme helps to minimize the numerical diffusion by reducing the net amount of fluxing. In addition, it saves total calculational time by providing resolution only where it is needed.

The code also has an iterative approach to the pressure accelerations to avoid the Courant limitation on the time step. A more complete description of the code is contained in the Appendix.

The wall of the system is given a constant, negative radial velocity at t = 0 and the subsequent evolution of the gas is computed. An artificial bulk viscosity is added to the system to render the evolution computationally tractable. The

equations are made dimensionless by normalizing lengths to the initial radius of the system, velocities to the adiabatic sound speed, and densities to the initial density at the center of the system. A matrix of nine cases was run, with $R = 0.6667a$ and $h = 0.0167a$, treating radial wall speed $|u_o|$ of 1/3, 1.0, and 3.0, and peak initial rotational speed v_o of 1/3, 1.0, and 3.0, spanning subsonic, sonic, and supersonic behavior in both speeds. The cases were run with an adiabatic exponent, $\gamma = 1.4$. A few test runs indicated that results depend weakly on values of γ provided that γ is not too near unity. Results are obtained with 43 mesh points in the radial direction and one zone in the theta direction. However, the validity of even fine points of the calculation was verified by refining the mesh in the radial direction to 73 points, by running with three or four zones in the theta direction, and by running at a variety of bulk viscosities.

We begin by discussing the results of the $|u_o| = v_o = 1/3$ case, as it is typical. Results are shown for u, v, and ρ in Figs. 1 and 2. Were the u velocity a linear function of r at all times, running from zero at the origin to $-u_o$ at the wall, the scaling laws of the previous section would hold exactly, the v profile would be preserved in time in a self-similar way, and the density profile would also. It is seen that the deviations of the u profile from linearity are substantial, but that the deviations of the v and ρ profiles from self-similar behavior are much smaller. This suggests that the u profiles are roughly fluctuating about the linear profile and that the scaling laws hold in a statistical sense, an idea that is approximately correct and which is quantified below.

We first comment on the qualitative aspects of the u profiles. Initially a strong shock communicates the motion of the wall to the rest of the gas. After the shock reaches the center of the system the velocity profile is, on the average, a linear one. There are, however, substantial deviations induced by shock propagation and by reflections from the center, from the wall, and from the density gradient in the body of the gas. In addition, the shock speed is variable in a density gradient, increasing at lower densities. Finally, we have several waves in the system simultaneously. Resonance effects then propagate disturbances at somewhat different rates than that of an elementary wave. Individual events are quite rapid in the u profiles - they require a time scale of $\Delta t \sim 0.01 - 0.02$ for resolution and are often over in $\Delta t \sim 0.06$ to 0.08.

For all of these reasons we have been unable to interpret individual propagation speeds or wave amplitudes in terms of the predictions of some analytical model. Accordingly, we have been much concerned with the question of the relia-

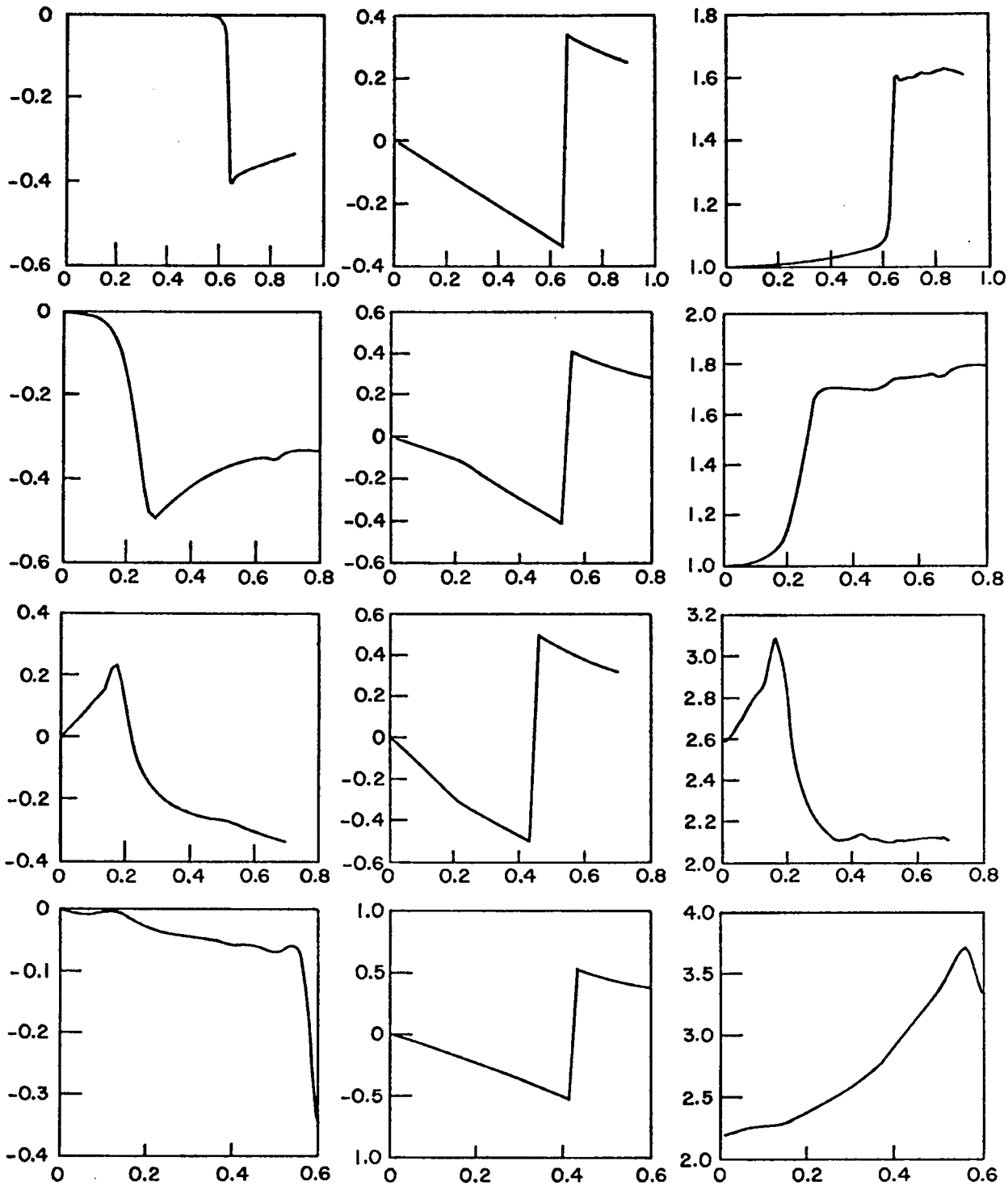

Fig. 1. u, v, and ρ vs r at t = 0.3, 0.6, 0.9, and 1.2 for $|u_o| = v_o = 1/3$.

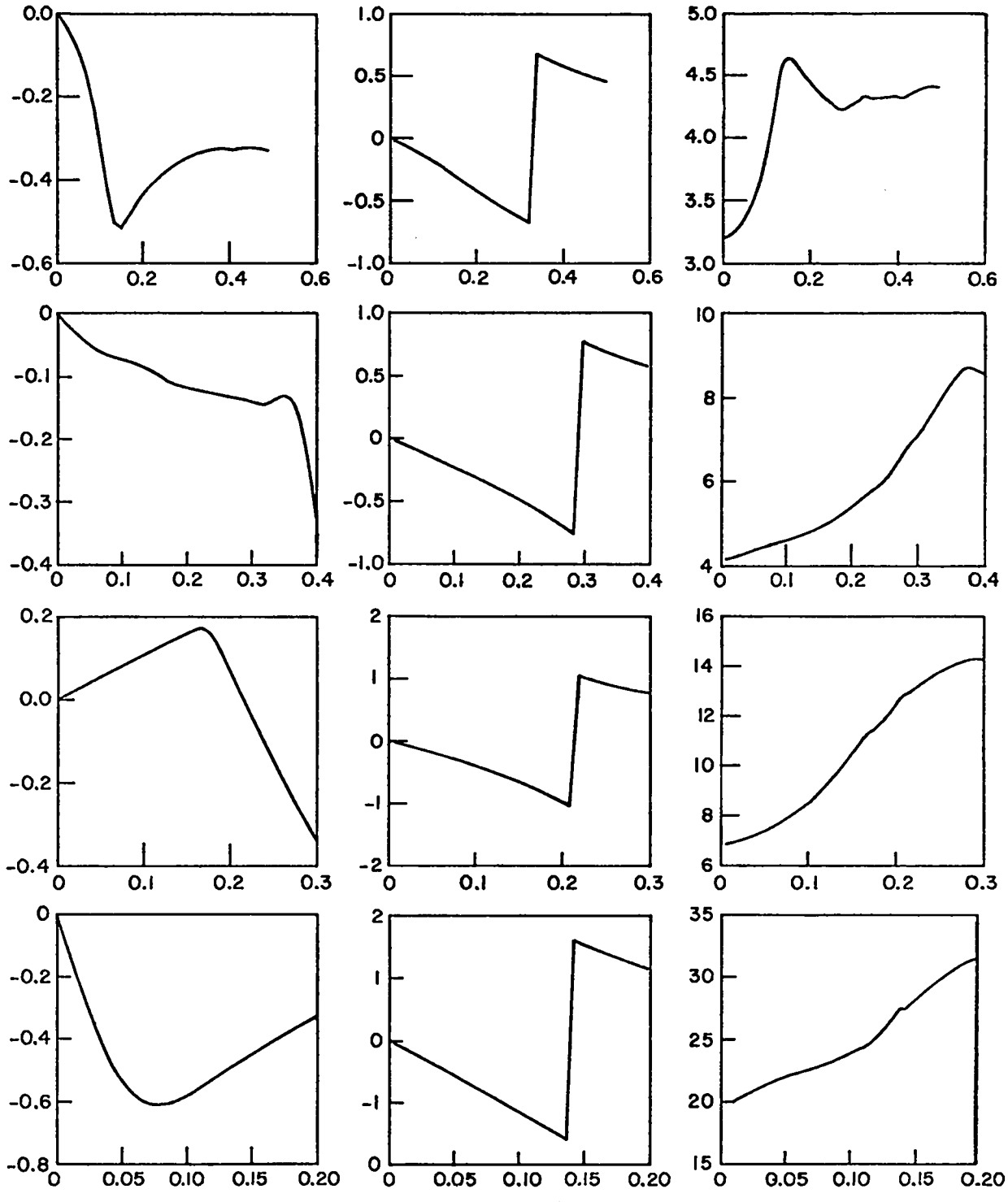

Fig. 2. u, v, and ρ vs r at t = 1.5, 1.8, 2.1, and 2.4 for $|u_o| = v_o = 1/3$.

bility of the computed details of these wave motions. As mentioned earlier, we have run the problem with a number of refinements and obtain virtually identical results, as long as the viscosity is not too large or the mesh too coarse, and we conclude that the details of the calculation are substantially correct. Further testing of the code on test problems where exact results exist would be welcome, however.

We quantify the notion of approximate scaling first by plotting $\varepsilon = [h(t)/R(t)]$ and $\Omega = [v_o(t)/2h(t)]$, two quantities basic to the instability theory presented below, against a(t) in Fig. 3. According to the scaling rules these quantities would vary as a^0 and a^2 respectively, and hence would yield straight lines on the log-log plots. We see that after an initial delay corresponding to propagation of the initial shock wave, the quantities do roughly oscillate about straight lines, although the ideal scaling law lines shown in Fig. 3 are not precisely equal to least squares lines through the data. Because of the rapid time variation of the

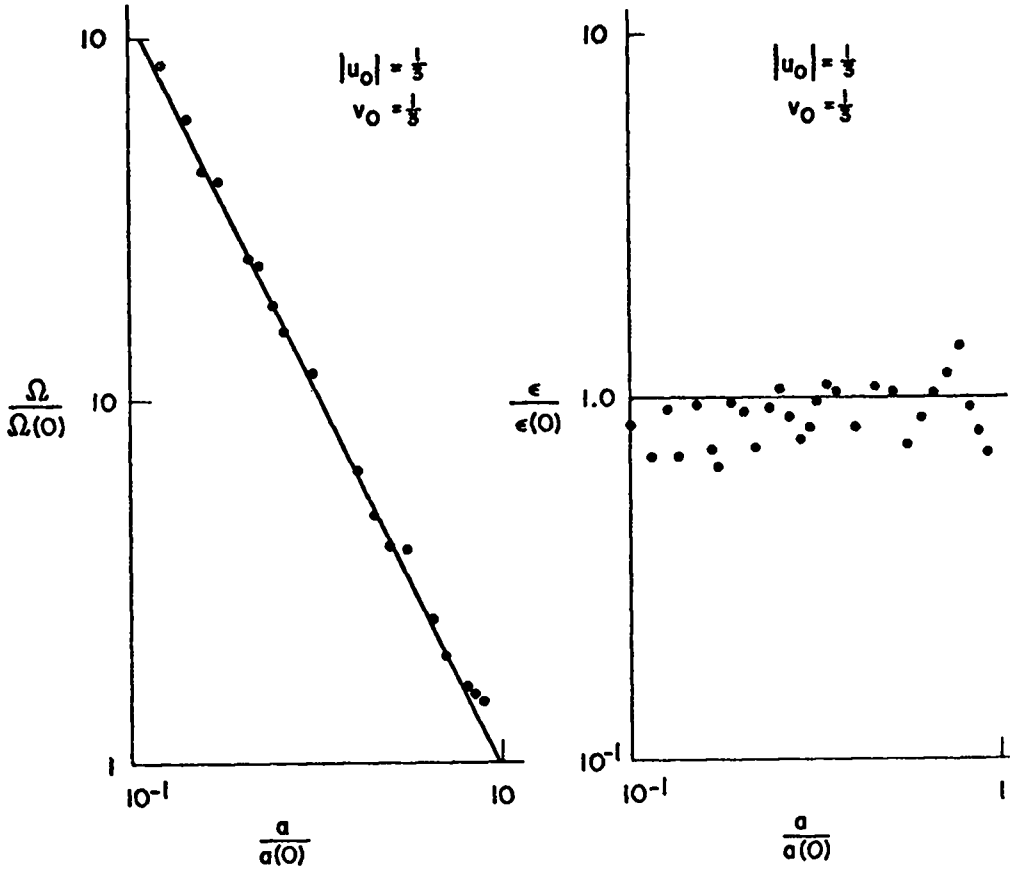

Fig. 3. Values of $\Omega/\Omega(o)$ and $\varepsilon/\varepsilon(o)$ vs $a/a(o)$ and comparison with the ideal.

oscillations and of the finite time resolution of the points of Fig. 3, the points of this figure resemble a scatter around a scaling law. Actually they are points appearing with constant frequency on a quasi-periodic oscillation about the scaling law.

We further quantify this notion by fitting each quantity to a formula of the form

$$\alpha \left[\frac{a(t)}{a(0)}\right]^n + \beta \quad .$$

The quantities α, β, and n are functions of time which at every linear compression ratio greater than 1.5 are determined by using a cumulative sum of points for a least squares fit. We obtain for Ω: $n = -2.06 \pm 0.13$, and for ε: $n = 0.26 \pm 0.10$. The quantities β are generally quite small, of order 10^{-2} and the α are of order unity. We see that there is approximate scaling. Though the scaling exponents do not agree precisely with the ideal laws proposed earlier, the ideal results are roughly within the scatter of the least squares exponents.

We display the least squares exponents for ε and Ω in Tables I and II for our matrix of cases. We see that the approximate scaling exponents are very close to the ideal scaling values. With the exception of the $|u_o| = 3$, $v_o = 3$ case, the results are consistent with the scaling exponents being independent of u_o and only weakly dependent on v_o. The exceptional case suggests that the weak dependence of the scaling exponents may actually be in the variable v_o/u_o. The evaluation of the approximate scaling exponents is an extremely sensitive test of an implosion calculation. Thus the consistency of the results obtained is strong evidence that the details of the shock propagation are being simulated correctly.

TABLE I

EXPONENTS n FOR $\Omega = v_o/2h$

v_o \ $\lvert u_o \rvert$	1/3	1.0	3.0
1/3	-2.06 ± 0.13	-1.94 ± 0.07	-2.07 ± 0.07
1.0	-2.32 ± 0.07	-2.18 ± 0.16	-2.17 ± 0.12
3.0	-2.50 ± 0.04	-2.44 ± 0.20	-1.97 ± 0.05

TABLE II

EXPONENTS n FOR $\varepsilon = h/R$

v_o \ $\lvert u_o \rvert$	1/3	1.0	3.0
1/3	0.26 ± 0.10	0.29 ± 0.11	0.14 ± 0.107
1.0	0.53 ± 0.07	0.43 ± 0.16	0.44 ± 0.15
3.0	0.68 ± 0.03	0.67 ± 0.26	0.52 ± 0.19

V. APPROXIMATE PERTURBATION THEORY FOR THE HELMHOLTZ INSTABILITY

We obtain perturbation equations for a cylindrically symmetric configuration of an incompressible fluid in which radial velocities are ignored and an azimuthal velocity profile is specified. Since we apply this theory to compressible fluids in which the radial velocities are larger than azimuthal velocities, a few words about our approximations are in order.

We make these approximations in this initial stage of the project primarily for mathematical simplicity but also to make direct contact with the very suggestive calculations of Greenspan and Benney. When the radial flow is subsonic, the compressibility of the fluid is not strongly excited and incompressible theory is not seriously in error. The radial flow is not in itself destabilizing - it affects the convective properties of the instability and the time available for any given fluid element to suffer an amplified disturbance when it passes through the unstable shear layer. But when the radial velocity is supersonic, substantial corrections to our theory can be expected because (1) the fluid compresses severely in the unperturbed flow, (2) the spatial extent of a shear-layer perturbation will be severely contracted when a shock wave passes through the shear-layer region, and (3) the propagation properties of supersonic flows limit the extent to which an amplifying disturbance can communicate the disturbance upstream. In such cases our theory can be expected to provide only qualitative information. The radial flow also produces Rayleigh-Taylor instability, which is not treated here.

We write the Euler equations for the azimuthal velocity profile specified previously, take the perturbed velocity field to be specified or, equivalently, take the perturbed radial velocity to be

$$u(r,\theta,t) = A(r,t)e^{im\theta} \quad ,$$

where

$$A(r,t) = a(t)r^{m-1} \qquad \text{for } r \leq R(t) - h(t) \ ,$$

$$= G(t)r^{m-1} + H(t)r^{-(m+1)} \qquad \text{for } R(t) - h(t) \leq r \leq R(t) + h(t) \ , \text{ and}$$

$$= E(t)r^{m-1} + F(t)r^{-(m+1)} \qquad \text{for } R(t) + h(t) \leq r \leq a(t) \ .$$

We require continuity of the pressure and the radial velocity at the two edges of the shear layer and demand that $u = u_o$ at $r = a(t)$. This yields two time evolution equations for the primary variables

$$\eta(t) = G(t)\ [R(t) + h(t)]^m$$

and

$$\chi(t) = H(t)\ [R(t) - h(t)]^{-m} \ ,$$

expressed in terms of previously defined quantities and in terms of

$$\varepsilon(t) = \frac{h(t)}{R(t)} \ , \quad J(t) = \frac{1-\varepsilon}{1+\varepsilon} \ , \quad K = J^m \ ,$$

$$S(t) = \frac{a(t)^{2m} + [R(t) + h(t)]^{2m}}{a(t)^{2m} - [R(t) + h(t)]^{2m}} \ , \text{ and } \quad \tau = \int_o^t dt'\ \Omega(t') \ .$$

The evolution equations are

$$\frac{d}{d\tau}\chi = i\left(\frac{2m\varepsilon}{1-\varepsilon} - J^{-1}\right)\chi - iJ^{-1}K\eta$$

$$\frac{d}{d\tau}\eta + 2\eta\frac{d}{d\tau}\ell n\ (1+S)$$

$$= -i\left(\frac{2m\varepsilon}{1+\varepsilon} - 1\right)\eta + iK\chi - \left(\frac{S-1}{S+1}\right)\left\{i\eta + K\frac{d}{d\tau}\chi\right.$$

$$\left. + i\left(\frac{2m\varepsilon}{1+\varepsilon} + 1\right)K\chi - mK\chi\frac{d}{d\tau}\ell n\ (R-h)\right\} \ ,$$

where the quantities involving S disappear in an infinite system.

Under the ideal scaling laws proposed earlier ε, J, K, and S are constant in τ and thus perturbed quantities oscillate and grow with the exponentiation rate

$$e^{c\tau} ,$$

where, for maximum growth, $c \sim 0.4$. Thus the main effect of the implosion is the contracted time scale inherent in the relation between t and τ. Using idealized scaling and assuming constant implosion speed u_o of the wall this becomes

$$\tau = \Omega(0) \left[\frac{a(0)}{a(t)}\right] t ,$$

so the exponentiation rate increases in order of magnitude during the implosion.

The disturbances predicted by our instability equations are remarkably similar to the predictions for the Helmholtz instability in plane geometry. For example, we have evaluated the slightly simpler dispersion relation obtained from a time-independent, infinite unperturbed system in which the outer fluid region is rigidly rotating for all values of m and ε and compared it to plane Helmholtz results for a shear layer of the same thickness 2h and same wavenumber $k = m/R$. Thus the plane results also may be plotted versus m, with ε as a parameter, and compared with graphs of the cylindrical results. This is done in Fig. 4 for a representative set of ε values. In these graphs c denotes the normalized cylindrical growth rate and f the value of

$$f = (c_{\text{cylindrical}}/c_{\text{plane}}) .$$

It is seen that the growth rates of the cylindrical and of the plane systems are virtually identical, even for shear layers which are 20% of their radius in thickness. It is conjectured that this similarity will persist into the nonlinear regime and the final result of this instability will be a ring of vortex tubes parallel to the system axis.

We may anticipate that realistic implosion calculations will yield fluctuating ε values as in Fig. 3 followed by a systematic shift to smaller ε's. This will give rise to phenomena similar to those reported by Greenspan and Benney as well as to a shift of the most unstable mode to higher m values as the implosion proceeds. Analogous effects in the τ vs t relation will also contribute to these

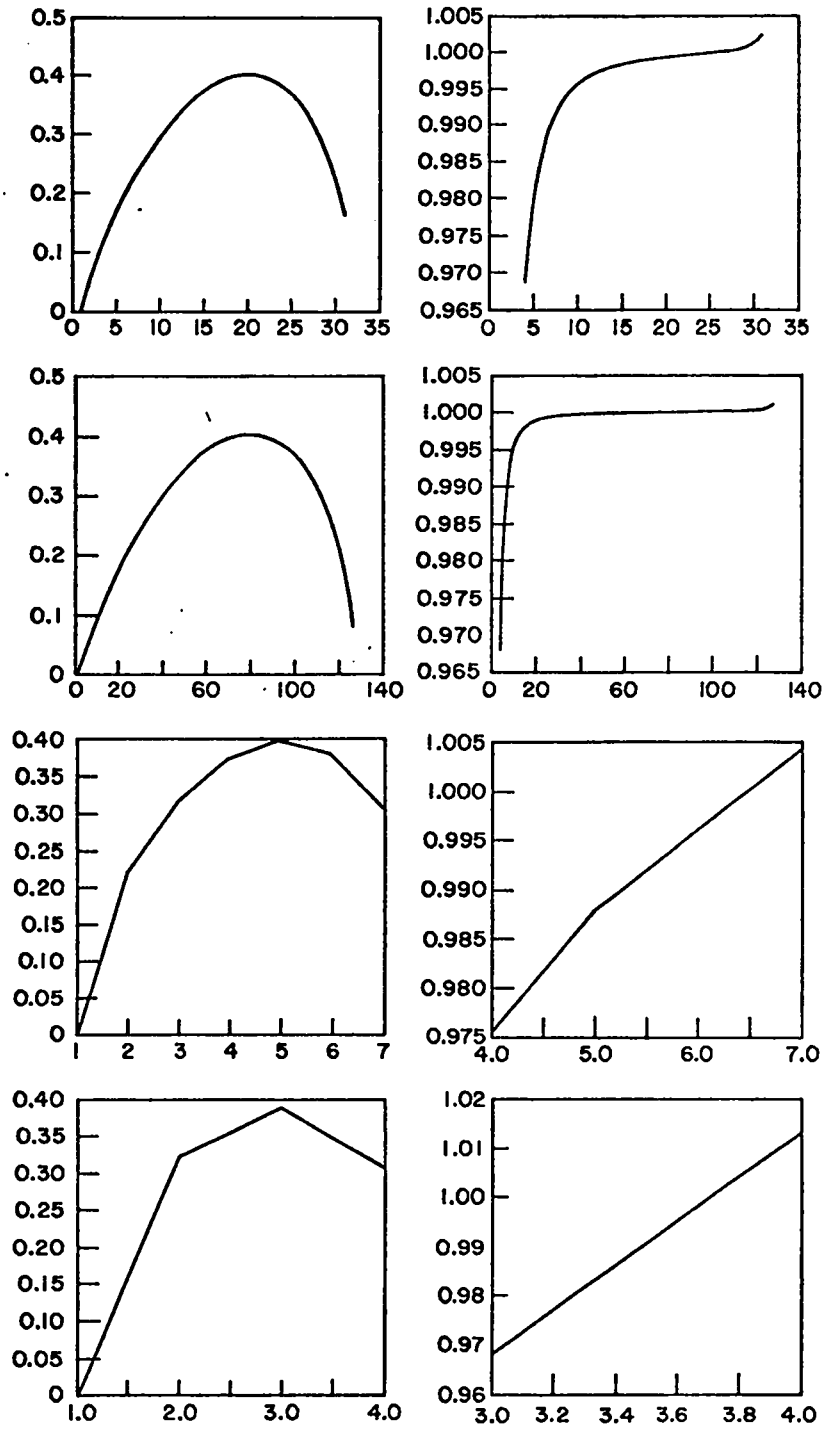

Fig. 4. Values of cylindrical Helmholtz instability growth rate c, and the ratio of c/c_{plane} vs m for values of the shear-layer thickness parameter ϵ 0.005, 0.02, 0.08, and 0.14.

results. As mentioned earlier, we anticipate that nonlinear effects may cause a widening of the shear layer and a shift to lower m values.

VI. CONCLUDING REMARKS

It is an open question whether the entire developmental sequence of the Helmholtz instability outlined above will be verified by ongoing work. The early stages of this work are favorable to our conjectures. But, in particular, it is not clear whether the entire developmental sequence will have time to occur.

APPENDIX

DESCRIPTION OF THE CODE

The usual set of equations for fluid flow can be differenced in such a way as to conserve angular momentum. We* have written such a code in polar coordinates and structured it with sufficient flexibility to provide several important and useful options. For one, the code can be run explicitly, that is the momentum equation is solved solely in terms of retarded time quantities. It can be run implicitly, the velocity field and pressure field are simultaneously advanced in time so that the Courant limit on the time step can be ignored.

For another, the code can be run either in the Eulerian mode or in a partially Lagrangian mode; partially because in this code the velocities are stored at cell faces and not at vertices as in a fully Lagrangian code. This disposition of the velocities implies certain constraints on the mesh movement which we shall detail below. These various options in any combination are easily selected by input parameters.

To achieve this flexibility the code is modularized in the following fashion: an explicit Lagrangian phase updates the velocities in terms of the pressures calculated in the previous cycle. The velocity field so obtained is then either a first guess for the pressure iteration, if the implicit option is elected, or the field with which the convection terms are calculated in the case of an

*This code was written in collaboration with Francis H. Harlow, who contributed the original ideas. His counsel throughout all stages of the work, from writing the code through the calculations reported herein, is gratefully acknowledged.

explicit calculation. If an implicit calculation is desired, the code goes through a Newton-Raphson iteration on the mass equation[3] to advance the pressure field at the same time as the velocities are updated. The iteration proceeds until an input convergence criterion is satisfied by the pressure changes. Having obtained the velocities, either explicitly or implicitly, one can choose between a number of rezone options to move the mesh each cycle.

Consider the mesh structure as shown in Fig. A-1. For a truly Lagrangian code where velocities are stored at cell vertices, there need be no restriction on the grid velocity. No matter what its value, all four cell edges will continue to intersect at a point, the cell vertex. With the configuration of Fig. A-1, this need not be so. For example, grid velocity $v_{g_{i,j+1}}$ different from the grid velocity $v_{g_{i,j}}$ will result in a displacement of the two cell edges relative to one another. In order for all four cell edges to continue to meet at a single point, it is necessary to require that all cell faces of a given radial index, j, be at a single radius after the grid motion has taken place. Similarly we must require that a given ray, i, must be at a single angle, θ, after the rezone. Within these constraints we allow the following options for the rezone in terms of the grid velocities u_g, v_g.

For the radial direction the grid velocity may be:

1) Purely Eulerian

$$u_g = 0 \ ;$$

2) Partially Lagrangian

$$u_{g,j} = \frac{1}{NTHE} \sum_i u_{i,j} \ ;$$

NTHE is the number of cells in the theta direction. This algorithm produces a different grid velocity in the radial direction for each row of cells, j. It has the advantage that it allows the mesh to move radially with a velocity that approximates the local fluid velocity. As such it minimizes the numerical diffusion normally associated with convection and it also allows regions of higher resolution to follow the fluid as it implodes or explodes;

3) Linearly scaled to an imposed piston velocity

$$u_{g,j} = \frac{(j-1)\ u_o}{NR} \ .$$

This achieves a linear profile of grid velocities in the radial direction scaled to the velocity applied at the outer boundary, u_o. NR is the number of cells in the radial direction.

Any of these can be combined with similar algorithms for the grid velocity in the θ-direction

4) Purely Eulerian

$$v_g = 0 \ ;$$

5) A single rotational velocity for the whole grid equal to the average rotation of the system (solid body rotation):

$$v_{g_{i,j}} = rc_{i,j} \left[\frac{1}{NR \times NTHE} \sum_{i',j'} \frac{v_{i',j'}}{rc_{i',j'}} \right] \ ;$$

6) A local theta velocity, fixed for each ray, perhaps equal to the average velocity along the ray.

$$v_{g_{i,j}} = \frac{rc_{i,j}}{NR} \sum_{j'} \frac{v_{i,j'}}{rc_{i,j'}} \ .$$

In the above equation rc is the radius at the center of the cell, the radius at which the azimuthal velocities are stored. (See Fig. A-1.) Having selected the grid velocities, we calculate a relative velocity,

$$\vec{u}_{rel} = \vec{u}_f - \vec{u}_g \ ,$$

where $\vec{u}_f$ is the fluid velocity at the end of the Lagrangian phase.

It is in terms of this relative velocity that the fluxing is calculated.

This outlines the basic code structure. The code contains also the option of adding numerical viscosity, of automatically calculating the time step to satisfy the relevant stability criteria, and of employing a full complement of output routines.

Turning to the manner in which the equations are differenced to ensure angular momentum conservation, we consider the momentum equation in the theta direction

$$\rho \frac{d(vr)}{dt} = - \frac{\partial p}{\partial \theta} + r \Lambda_\theta \ .$$

The last term, r Λ_θ, contains all the viscous additions. We integrate this equation over the control volume as indicated in Fig. A-2

$$\int \frac{\partial p}{\partial \theta}\, d\tau = \int_{r_{i,j}}^{r_{i,j+1}} rdr\, [p_{i,j} - p_{i-1,j}] = (p_{i,j} - p_{i-1,j})\, \frac{\left(r^2_{i,j+1} - r^2_{i,j}\right)}{2}$$

$$= (p_{i,j} - p_{i-1,j})\, rc_{i,j}\, \delta r \quad .$$

Note that the equation for the velocity in the azimuthal direction has been written in terms of changes in the quantity vr, in which r is the time varying coordinate of the fluid element. This and the above limits of integration are to be distinguished from the independent Lagrangian coordinate that appears in the integrand. The form of this momentum equation arises naturally from a derivation that combines the coriolis and convective terms into an angular momentum conserving form, which is then transferred into the Lagrangian frame. This is crucial to the goal of angular momentum conservation. Summing the above difference expression over a row of cells shows clearly that this form conserves angular momentum. Similarly, we have written the difference expressions for the viscous accelerations and the convection terms for the quantity vr in such a way as to conserve the total angular momentum in the system. One can readily show that the price one pays is that linear momentum is no longer conserved.

None of the above makes any assumption as to the equation of state used. The pressures are separately calculated by any prescription required. We have generally specialized in our test problems to a simple form for p,

$$p = a^2(\rho - \rho_o) + (\gamma - 1)\, \rho I \quad ,$$

where a^2, ρ_o, and γ-1 are input quantities. The specific internal energy, I, can be calculated from the usual expression

$$\rho \frac{dI}{dt} = - p\, \nabla \cdot \vec{u} + \text{viscous terms.}$$

If p does not depend on I, the calculation of specific internal energy is omitted.

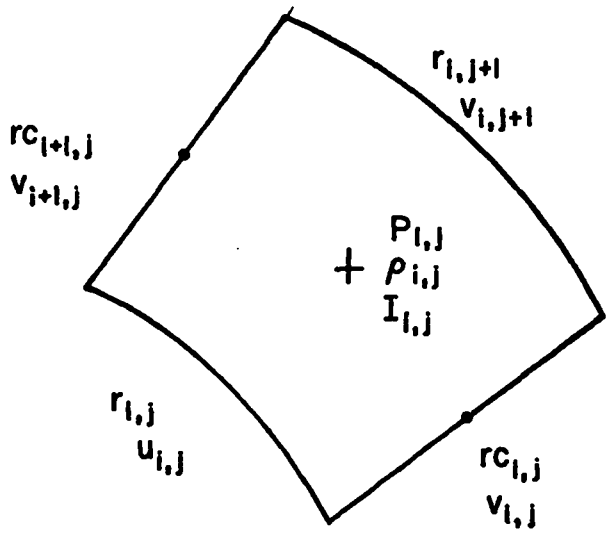

Fig. A-1. Location of variables on cell faces and at cell center.

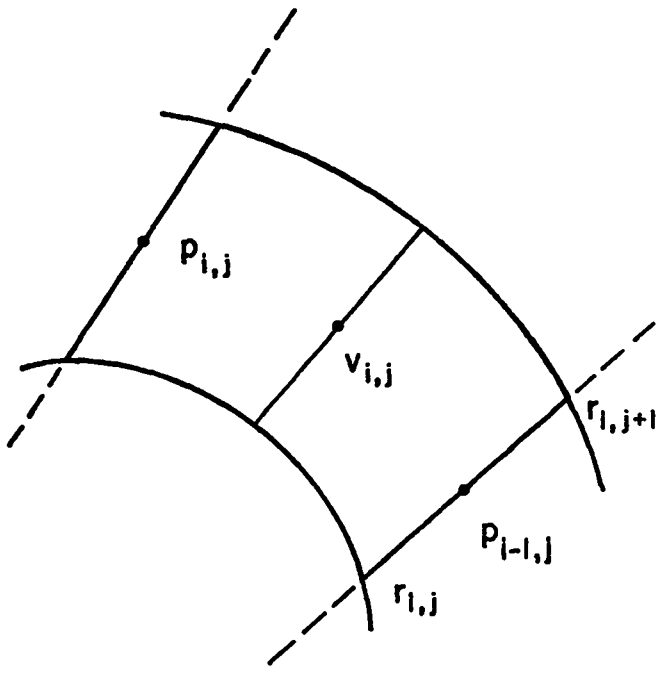

Fig. A-2. Control volume to calculate pressure accelerations.

REFERENCES

1. H. P. Greenspan and D. J. Benney, "On Shear-Layer Instability, Breakdown and Transition," J. Fluid Mech. 15, 133 (1963).

2. C. W. Hirt, A. A. Amsden, and J. L. Cook, "An Arbitrary Lagrangian-Eulerian Computing Method for All Flow Speeds," J. Comp. Phys. 14, 227 (1974).

3. A. A. Amsden and C. W. Hirt, "YAQUI: An Arbitrary Lagrangian-Eulerian Computing Method for All Flow Speeds," Los Alamos Scientific Laboratory report, LA-5100 (1973).